

---

# Only Bayes should learn a manifold

(on the estimation of differential geometric structure from data)

---

**Søren Hauberg**  
Section for Cognitive Systems  
Technical University of Denmark  
sohau@dtu.dk

## Abstract

We investigate learning of the differential geometric structure of a data manifold embedded in a high-dimensional Euclidean space. We first analyze kernel-based algorithms and show that under the usual regularizations, non-probabilistic methods cannot recover the differential geometric structure, but instead find mostly linear manifolds or spaces equipped with teleports. To properly learn the differential geometric structure, non-probabilistic methods must apply regularizations that enforce large gradients, which go against common wisdom. We repeat the analysis for probabilistic methods and find that under reasonable priors, the geometric structure can be recovered. Fully exploiting the recovered structure, however, requires the development of stochastic extensions to classic Riemannian geometry. We take early steps in that regard. Finally, we partly extend the analysis to modern models based on neural networks, thereby highlighting geometric and probabilistic shortcomings of current deep generative models.

Comments on this document are gratefully accepted at sohau@dtu.dk

## 1 Introduction

*Manifold learning* as a concept comes in many forms. Some techniques seek a low-dimensional embedding of high-dimensional data such as to preserve certain aspects of the data. This line of thinking includes classic methods such as *Isomap* [20], *Locally linear embeddings* [16], *Laplacian eigenmaps* [2] and more [18, 4]. Probabilistic methods often view the underlying data manifold as governed by a latent variable along with a generative model that describe how the latent manifold is to be embedded in the data space. The common theme is the quest for a low-dimensional representation of the data, which can be visualized or otherwise utilized to find a solution to a given task.

Ideally, we want an *operational representation*, i.e. we want to be able to make mathematically meaningful calculations with respect to the learned low-dimensional representation. We argue that a good representation should at least support the following operations:

- **Interpolation:** given two points, it should be possible to derive a natural and unique interpolating curve that follow the manifold.
- **Distances:** given two points, their distance should be well-defined and (informally) reflect the amount of energy required to transform one point to another.
- **Measure:** the representation should be equipped with a measure under which integration is well-defined for all points on the manifold.

These are elementary requirements of a representation, yet most manifold learning schemes do not deliver.

Preprint. Work in progress.

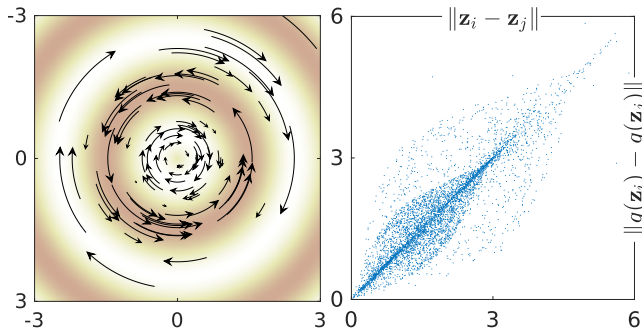


Figure 1: Reparametrizations illustrated. The left panel shows a “swirling” transformation of  $\mathcal{Z}$  with the property that a Gaussian variable with zero mean and unit covariance, will have the same distribution after a reparametrization. The right panel shows pair-wise distances between points before and after reparametrization; evidently the geometry of  $\mathcal{Z}$  is sensitive to reparametrizations.

**Embedding methods** seek a low-dimensional embedding  $\mathbf{z}_{1:N} = \{\mathbf{z}_1, \dots, \mathbf{z}_N\}$  of the original data  $\mathbf{x}_{1:N}$ . These methods fundamentally only describe the data manifold at the points where data is observed and nowhere else. As such, the low-dimensional embedding space is only well-defined at  $\mathbf{z}_{1:N}$ . It is common to treat the low-dimensional embedding space as being Euclidean, but this will always be a *post hoc* assumption with limited grounding in the actual embedding method. Fundamentally, the learned representation space is a discrete space that does not lend itself to continuous interpolations. Likewise, the most natural measure of such a discrete space will only assign mass to the points  $\mathbf{z}_{1:N}$ , and any distribution with respect to such a measure will also be discrete. This is perhaps too limiting to fit our needs.

**Generative models** estimate a set of low-dimensional latent variables  $\mathbf{z}_{1:N}$  along with a suitable mapping  $f : \mathcal{Z} \rightarrow \mathcal{X}$  such that  $f(\mathbf{z}) \approx \mathbf{x}$ . It is, again, common to treat the latent space  $\mathcal{Z}$  as being Euclidean. However, this assumption easily lead to arbitrariness. As an example, consider the *variational autoencoder (VAE)* [8, 15], which seek a representation in which  $\mathbf{z}_{1:N}$  follow a unit Gaussian distribution. Now consider the transformation  $g(\mathbf{z}) = \mathbf{R}_\theta \mathbf{z}$ , where  $\mathbf{R}_\theta$  is a linear transformation that rotate points by  $\theta(\mathbf{z}) = \sin(\pi\|\mathbf{z}\|)$ . This is a smooth invertible transformation with the property that  $\mathbf{z} \sim \mathcal{N}(\mathbf{0}, \mathbf{I}) \Rightarrow g(\mathbf{z}) \sim \mathcal{N}(\mathbf{0}, \mathbf{I})$ . The transformation is shown in Fig. 1. If the latent variables  $\mathbf{z}_{1:N}$  and the generator  $f$  is an optimal VAE, then  $g(\mathbf{z}_{1:N})$  and  $g^{-1} \circ f$  is equally optimal. Yet, the latent spaces  $\mathcal{Z}$  and  $g(\mathcal{Z})$  are quite different; Fig. 1 shows the Euclidean distances between  $\mathbf{z}_n$  and  $g(\mathbf{z}_n)$  for samples drawn from a unit Gaussian. We, unsurprisingly, see that the transformed latent space is significantly different from the original space. As the VAE provides no guarantees as to which latent space is recovered, we must be careful when relying on the Euclidean latent space: distances between points are essentially arbitrary and as are straight-line interpolations. Any analysis relying on vector operations in the latent space are, thus, arbitrary as well, and positive result from such operations should be viewed as pure luck with little mathematical grounding. Ideally, we want a representation space that is invariant to such transformations, but current models do not provide such invariances.

**In this paper**, we consider models where the representation space  $\mathcal{Z}$  is learned jointly with a smooth mapping  $f : \mathcal{Z} \rightarrow \mathcal{X}$ , such that  $\mathcal{Z}$  can naturally be endowed with a Riemannian metric (Sec. 2). This gives a representation space with natural interpolants corresponding to shortest paths along the learned manifold in  $\mathcal{X}$ . Distances are then the length of such shortest paths. Furthermore, the representation space is naturally equipped with a measure such that integration is straight-forward, implying that distributions can be defined in  $\mathcal{Z}$ . We contribute a detailed analysis of the case where  $f$  is estimated by a kernel method (Sec. 3), and show that even in the case of infinite noise-free data a non-probabilistic estimate of  $f$  cannot recover the true Riemannian structure of  $\mathcal{Z}$ . In contrast, probabilistic estimates of  $f$  can indeed recover the true Riemannian structure (Sec. 4). Fully exploiting this structure, however, require the development of Bayesian extensions to classic differential geometry (Sec. 5); we contribute elementary results in that regard, but many questions remain open. Finally, we partly extend our analysis to the setting where  $f$  is estimated by a neural network and demonstrate that deep generative models are still lacking elementary properties before they can learn the Riemannian structure of data manifolds (Sec. 6).

**Notation.** Throughout the paper,  $\mathcal{Z}$  denote the  $d$ -dimensional *representation* or *latent space*, which is learned from data in the *observation space*  $\mathcal{X} \equiv \mathbb{R}^D$ . Latent points are denoted  $\mathbf{z}_n \in \mathcal{Z}$ , while corresponding observations are  $\mathbf{x}_n \in \mathcal{X}$ . The mapping  $f : \mathcal{Z} \rightarrow \mathcal{X}$  embeds  $\mathcal{Z}$  in  $\mathcal{X}$ ; we denote  $\mathcal{M} = f(\mathcal{Z})$  and assume that  $\mathcal{M}$  is a Riemannian manifold (see Sec. 2).

## 2 A short primer on Riemannian manifolds

A  $d$ -dimensional manifold  $\mathcal{M}$  embedded in  $\mathbb{R}^D$  ( $d < D$ ) is a topological space in which there exist a neighborhood around each point  $\mathbf{x} \in \mathcal{M}$  that is homeomorphic to  $\mathbb{R}^d$  [5]. Informally,  $\mathcal{M}$  is a (usually nonlinear) surface in  $\mathbb{R}^D$  that is locally Euclidean, i.e. it does not self-intersect or otherwise locally change dimensionality, etc. We assume that we have a  $d$ -dimensional parametrization<sup>1</sup>  $\mathcal{Z}$  of the manifold along with a mapping  $f : \mathcal{Z} \rightarrow \mathcal{X}$ , such that  $\mathcal{M} = f(\mathcal{Z})$ .

We start our discussion by defining the inner product between points in  $\mathbb{R}^D$  as  $\langle \mathbf{x}, \mathbf{x}' \rangle = 1/D \sum_i x_i x'_i$ . The division by  $D$  ensures that this inner product converge to the usual  $l_2$  inner product in the limit  $D \rightarrow \infty$ . Now, let  $\mathbf{z}$  be a  $d$ -dimensional latent point and let  $\Delta_1$  and  $\Delta_2$  be infinitesimals, then we can compute their inner product around  $\mathbf{z}$  in the data space using Taylor's Theorem,

$$\langle f(\mathbf{z} + \Delta_1) - f(\mathbf{z}), f(\mathbf{z} + \Delta_2) - f(\mathbf{z}) \rangle = \langle f(\mathbf{z}) + \mathbf{J}_z \Delta_1 - f(\mathbf{z}), f(\mathbf{z}) + \mathbf{J}_z \Delta_2 - f(\mathbf{z}) \rangle \quad (2.1)$$

$$= \langle \mathbf{J}_z \Delta_1, \mathbf{J}_z \Delta_2 \rangle = 1/D \cdot \Delta_1^\top (\mathbf{J}_z^\top \mathbf{J}_z) \Delta_2, \quad (2.2)$$

where  $\mathbf{J}_z = \partial_{\mathbf{z}} f \in \mathbb{R}^{D \times d}$  is the Jacobian of  $f$  at  $\mathbf{z}$ . The  $d \times d$  symmetric positive definite matrix  $1/D \cdot \mathbf{J}_z^\top \mathbf{J}_z$ , thus defines a local inner product. We denote this matrix  $\mathbf{M}_z$  and refer to it as the (*pull-back*) *metric* of the manifold. Note that this local inner product is invariant to reparametrizations of the manifold as it merely correspond to the inner product of  $\mathcal{X}$  measured locally on the manifold. This inner product, thus, avoids the arbitrary parametrization issue discussed in the introduction.

Given a smooth curve  $\mathbf{c} : [a, b] \rightarrow \mathcal{Z}$ , we can measure its length under the local inner product as

$$\mathcal{L}(\mathbf{c}) = \int_a^b \sqrt{\dot{\mathbf{c}}_t^\top \mathbf{M}_{\mathbf{c}_t} \dot{\mathbf{c}}_t} dt, \quad (2.3)$$

where  $\dot{\mathbf{c}}_t = \partial_t \mathbf{c}(t)$  is the derivative (velocity) of the curve. Natural interpolants can then be defined as length minimizing curves connecting two points. Such a curve is known as a *geodesic*, and its length constitutes a natural distance measure along the manifold. Unfortunately, minimizing curve length gives rise to a poorly determined optimization problem as the length of a curve is invariant to its parametrization. The following classic proposition provides remedy to this situation [5]:

**Proposition 1.** *Let  $\mathbf{c} : [a, b] \rightarrow \mathcal{Z}$  be a smooth curve that (locally) minimize the curve energy*

$$\mathcal{E}(\mathbf{c}) = \frac{1}{2} \int_a^b \dot{\mathbf{c}}_t^\top \mathbf{M}_{\mathbf{c}_t} \dot{\mathbf{c}}_t dt, \quad (2.4)$$

*then  $\mathbf{c}$  has constant velocity and is (locally) length-minimizing.*

This energy functional is locally uniformly convex and therefore its solution is locally unique. Standard calculus of variation shows that curves of minimal energy satisfy the following system of second order differential equations,

$$\ddot{\mathbf{c}}_t = -\frac{1}{2} \mathbf{M}_{\mathbf{c}_t}^{-1} \left[ 2(\mathbf{I} \otimes \dot{\mathbf{c}}_t^\top) \partial_{\mathbf{c}_t} \text{vec}[\mathbf{M}_{\mathbf{c}_t}] \dot{\mathbf{c}}_t - \partial_{\mathbf{c}_t} \text{vec}[\mathbf{M}_{\mathbf{c}_t}]^\top (\dot{\mathbf{c}}_t \otimes \dot{\mathbf{c}}_t) \right], \quad (2.5)$$

where  $\text{vec}[\cdot]$  stacks the columns of a matrix into a vector and  $\otimes$  is the Kronecker product. Such systems can be solved numerically using standard techniques. Figure 2 gives an example geodesic.

Given a function  $h : \mathcal{X} \rightarrow \mathbb{R}$  we can integrate it over a part of the manifold  $f(\Omega)$  as

$$\int_{f(\Omega)} h(\mathbf{x}) d\mathbf{x} = \int_{\Omega} h(f(\mathbf{z})) \sqrt{\det(\mathbf{M}_z)} d\mathbf{z}. \quad (2.6)$$

The quantity  $\sqrt{\det(\mathbf{M})}$  is often known as the *Riemannian volume measure* and is akin to the Jacobian-determinant appearing in the *change of variables theorem*.

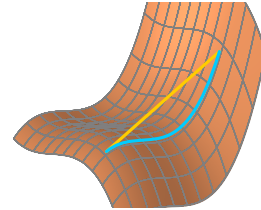


Figure 2: Geodesic interpolation along the manifold (blue) versus along a straight line (yellow).

<sup>1</sup>In mathematics, this is generally known as a *chart*; here we stick to the machine learning terminology.

### 3 Manifold learning with kernels

We now consider data  $\mathbf{x}_{1:N}$  distributed on a compact  $d$ -dimensional Riemannian submanifold  $\mathcal{M} \subset \mathbb{R}^D$  embedded in the data space. We consider a known set of  $d$ -dimensional representations  $\mathbf{z}_{1:N}$  and estimate the mapping  $f : \mathcal{Z} \rightarrow \mathcal{X}$  using different kernel methods. Note that this manifold is only locally diffeomorphic to  $d$ -dimensional Euclidean space, and it may globally self-intersect. For the sake of analysis, we assume noise-free data and consider the limit  $N \rightarrow \infty$ . This simple setting is sufficient to prove our main point, but the analysis also hold for noisy data.

Our key question is if we can recover the true Riemannian structure of  $\mathcal{Z}$  in this setting. Methods that fail at this given infinite noise-free data should generally be avoided. To perform the analysis, we will study the metric in regions that are near the training data, and in regions that are far away from the training data. We formalize these notions as follows.

**Definition 1.** For a point  $\mathbf{z}$  and a dataset  $\mathbf{Z}$ , the distance between them is

$$\text{dist}(\mathbf{z}, \mathbf{Z}) = \inf_{\tilde{\mathbf{z}} \in \mathbf{Z}} \|\mathbf{z} - \tilde{\mathbf{z}}\|. \quad (3.1)$$

Note that this infimum always exist as the element-wise distance is bounded from below by 0.

**Definition 2.** For a function  $\mathbf{x} = h(\mathbf{z})$ , we define the limit

$$\mathbf{x} \xrightarrow{\text{away}} \hat{\mathbf{x}} \quad (3.2)$$

if for any sequence  $\hat{\mathbf{z}}_l$  such that  $\text{dist}(\hat{\mathbf{z}}_l, \mathbf{Z}) \xrightarrow{l \rightarrow \infty} \infty$ , we have  $h(\hat{\mathbf{z}}_l) \xrightarrow{l \rightarrow \infty} \hat{\mathbf{x}}$ . Note that this latter limit is generally not defined. Similarly, we define

$$\mathbf{x} \xrightarrow{\text{near}} \hat{\mathbf{x}} \quad (3.3)$$

if for any sequence  $\hat{\mathbf{z}}_l$  such that  $\text{dist}(\hat{\mathbf{z}}_l, \mathbf{Z}) \xrightarrow{l \rightarrow \infty} 0$ , we have  $h(\hat{\mathbf{z}}_l) \xrightarrow{l \rightarrow \infty} \hat{\mathbf{x}}$ . Again, note that this latter limit is generally not defined.

#### 3.1 A guiding example

To illustrate the main point of the paper, we consider a simple guiding example. We draw data uniformly on a unit circle and nonlinearly embed it in  $\mathcal{X} = \mathbb{R}^{1000}$  with added Gaussian noise. Next we embed the data using PCA in  $\mathcal{Z} = \mathbb{R}^2$  and learn a mapping  $f$  from  $\mathcal{Z}$  to  $\mathcal{X}$ . Finally, we compute shortest paths under the pull-back metric; if the true metric is recovered we should see shortest paths corresponding circular arcs in  $\mathcal{Z}$ . Figure 3 show the corresponding points in  $\mathcal{Z}$ .

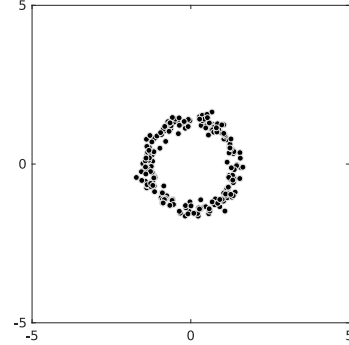


Figure 3: The latent points  $\mathbf{z}_n \in \mathcal{Z}$  for our guiding example.

#### 3.2 The deterministic setting

We now consider learning the mapping  $f : \mathcal{Z} \rightarrow \mathcal{X}$  using *kernel ridge regression* [17], i.e.

$$f_{\text{kr}}(\mathbf{z}_*) = k_{*,\mathbf{z}} (k_{\mathbf{z},\mathbf{z}} + \sigma^2 \mathbf{I})^{-1} \mathbf{x}_{1:N}, \quad (3.4)$$

where  $k$  is a suitable kernel function, and we have used the short-hand notations  $k_{*,\mathbf{z}} = k(\mathbf{z}_*, \mathbf{z}_{1:N}) \in \mathbb{R}^{1 \times N}$  and  $k_{\mathbf{z},\mathbf{z}} = k(\mathbf{z}_{1:N}, \mathbf{z}_{1:N}) \in \mathbb{R}^{N \times N}$ . The parameter  $\sigma^2$  encodes the uncertainty of  $\mathbf{x}_{1:N}$ ; to simplify analysis, we consider noise-free data and have  $\sigma^2 = 0$ . The pull-back metric associated with this regression function is then

$$\mathbf{M}_{\text{kr}}(\mathbf{z}_*) = \partial_{\mathbf{z}_*} k_{*,\mathbf{z}} k_{\mathbf{z},\mathbf{z}}^{-1} \mathbf{X} \mathbf{X}^\top k_{\mathbf{z},\mathbf{z}}^{-1} \partial_{\mathbf{z}_*} k_{*,\mathbf{z}}^\top, \quad (3.5)$$

where  $\mathbf{X} \in \mathbb{R}^{N \times D}$  are  $\mathbf{x}_{1:N}$  stacked as matrix. Assuming a universal kernel [17], then  $f_{\text{kr}}$  will correspond to the true mapping where we have data when  $N \rightarrow \infty$ . Consequently, we recover the true metric where we have data, i.e.  $\mathbf{M}_{\text{kr}} \xrightarrow{\text{near}} \mathbf{M}_{\text{true}}$ .

**Teleports?** The behavior away from data depend on the choice of kernel. We first consider the usual Gaussian kernel

$$k_{\text{RBF}}(\mathbf{z}, \mathbf{z}') = \theta_{\text{RBF}} \cdot \exp\left(-\frac{\alpha}{2}\|\mathbf{z} - \mathbf{z}'\|^2\right), \quad (3.6)$$

and note that similar observations hold for most common stationary kernels. From this, we see that

$$f_{\text{RBF}} \xrightarrow{\text{away}} \mathbf{0} \quad \text{and} \quad \mathbf{M}_{\text{RBF}} \xrightarrow{\text{away}} \mathbf{0}. \quad (3.7)$$

To understand the geometric implication of this observation, we consider our guiding example (Sec. 3.1). We compute shortest paths under the pull-back metric; if the true metric is recovered we should see shortest paths corresponding circular arcs in  $\mathcal{Z}$ . Figure 4 show the recovered geodesics (the background color is proportional to the volume measure); we see that shortest paths systematically shy away from the data and generally do not resemble circular arcs. The explanation is simple: in regions of  $\mathcal{Z}$  where the metric is zero geodesics do not increase in length. In terms of length-minimization, it is, thus, “free” to move through regions where the metric is zero. The result in Eq. 3.7, thus, implies that geodesics are encouraged to move away from the data. Intuitively, we can think of regions in  $\mathcal{Z}$  without data as “teleports” that points can move freely between. This also hold true, when the manifold is densely sampled, and consequently geodesics will generally not move along the data manifold, and the manifold geometry is not recovered.

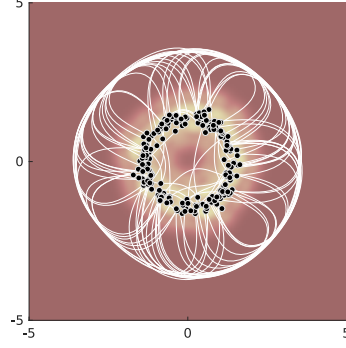


Figure 4: Geodesics for Gaussian kernel ridge regression. These are pushed away from the data through “teleports”.

**Flat manifolds?** These teleports are due to the fact that the chosen kernel cause the regression to extrapolate to a constant. This is perhaps a too simplistic setting, and we move on to a kernel that extrapolate linearly,

$$k_{\text{RBF+lin}}(\mathbf{z}, \mathbf{z}') = k_{\text{RBF}}(\mathbf{z}, \mathbf{z}') + \theta_{\text{lin}} \mathbf{z}^\top \mathbf{z}'. \quad (3.8)$$

Similarly to before, we see

$$f_{\text{RBF+lin}} \xrightarrow{\text{away}} \theta_{\text{lin}} \mathbf{z}_*^\top \mathbf{Z} k_{\mathbf{z}, \mathbf{z}}^{-1} \mathbf{X} = \mathbf{z}_*^\top \mathbf{B}, \quad (3.9)$$

where  $\mathbf{B} = \theta_{\text{lin}} \mathbf{Z} k_{\mathbf{z}, \mathbf{z}}^{-1} \mathbf{X} \in \mathbb{R}^{d \times D}$ . This amounts to linear extrapolation, as expected. When we move away from the data, the metric then becomes

$$\mathbf{M}_{\text{RBF+lin}} \xrightarrow{\text{away}} \mathbf{B} \mathbf{B}^\top. \quad (3.10)$$

This is a (scaled) Euclidean metric, implying that the learned manifold is flat in regions where we do not have data. As the pull-back metric measure distances in  $\mathcal{X}$ , where straight lines are shortest curves, then geodesics on the learned manifold will be encouraged to go through the flat regions where data is missing. This is also evident in Fig. 5 that shows the results of our guiding example. Here we see that geodesics are almost straight lines, implying that the learned manifold did not recover the structure of the data.

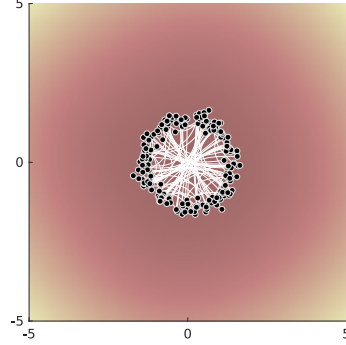


Figure 5: Geodesics for kernel ridge regression with a Gaussian+linear kernel. The linear extrapolation implies (almost) linear geodesics.

**An unstable solution?** We have so far seen that the traditional constant and linear extrapolation schemes imply that we cannot learn the correct geometry: either we introduce teleports or we learn mostly flat manifolds. We now reverse the question and ask: *how should we extrapolate in order to learn the correct geometry?* For geodesics to stay on the manifold, we informally need

$$\mathbf{M} \xrightarrow{\text{away}} [\text{sufficiently large}]. \quad (3.11)$$

That is, to ensure that geodesics always stay on the manifold, length-minimization must be penalized sufficiently for leaving the manifold. We, currently, do not have a tight bound on how large the metric must be to ensure this, though a loose bound is provided by the radius of the manifold. That is, let

$$r = \sup_{\mathbf{z}, \mathbf{z}' \in \mathcal{M}} \text{dist}(\mathbf{z}, \mathbf{z}') \quad (3.12)$$

denote the largest distance between points on the manifold, then geodesics stay on the manifold if

$$\lambda_{\min}(\mathbf{M}_{\text{sufficient}}) \xrightarrow{\text{away}} r^2. \quad (3.13)$$

Here  $\lambda_{\min}$  denote the function returning the smallest eigenvalue of a matrix. In differential geometry, it is common to call *any* locally length-minimizing curve a geodesic. Here we mean the shortest geodesic. To ensure that *all* locally length-minimizing curves stay on the manifold, we have no tighter bound than

$$\lambda_{\min}(\mathbf{M}_{\text{ideal}}) \xrightarrow{\text{away}} \infty. \quad (3.14)$$

If the metric must extrapolate to a large matrix, then the Jacobian  $\mathbf{J}$  must also extrapolate to a large matrix (since  $\mathbf{M} \propto \mathbf{J}^\top \mathbf{J}$ ). This, in turn, implies that whichever regression function we estimate must have large derivatives away from the data. This goes against common wisdom as a regression function with this property will generally not provide a particularly smooth interpolation of finite data.

**Summarizing discussion.** Most common choices for estimating  $f$  will ensure that the geometry of  $\mathcal{M}$  is well-estimated near the data, so the key factor to determine if we can well-estimate the manifold geometry is the behavior of  $f$  away from the data. In these regions, we depend on prior assumptions on  $f$  to determine the geometry. The most common (and sensible) choice of prior assumptions are related to the smoothness of  $f$  [7]. We have seen that the smoother assumptions we are willing to make, the more geodesics are drawn away from the data (“off the manifold”, so to say). The phenomenon is easily understood by considering a data manifold with a hole. If the applied regression function is very smooth, then the hole will be interpolated almost linearly, which imply that shortest paths along the manifold will cross over the hole. In the end, we are, thus, left with a simple choice: *either give up on learning the manifold geometry correctly* (by assuming  $f$  is very smooth) or *give up on staple learning* (by assuming  $f$  is non-smooth). Neither choice is desirable.

## 4 The Bayesian setting

We now move on to the setting where  $f$  is a probabilistic mapping. To make the discussion explicit, we consider the natural extension of the previously considered kernel ridge regression and let  $f$  consist of component-wise conditionally independent Gaussian processes,

$$f_i(\mathbf{z}) \sim \mathcal{GP}(m_i(\mathbf{z}), k(\mathbf{z}, \mathbf{z}')), \quad \forall i = 1, \dots, D. \quad (4.1)$$

This is the *Gaussian Process latent variable model (GP-LVM)* [11]. Here  $m_i$  and  $k$  are the mean and covariance functions of the  $i^{\text{th}}$  GP. Note that, like Lawrence [11], we assume the same covariance function across all dimensions as this simplifies future calculations. The geometry associated with this model was first studied by Tosi et al. [21]; several results in this section stem from that work.

The pull-back metric  $\mathbf{M} = 1/D \mathbf{J}^\top \mathbf{J}$  is now a stochastic Riemannian metric since  $f$  is stochastic. As Gaussian variables are closed under differentiation, then  $\mathbf{J}$  follows a GP,

$$\mathbf{J} \sim \prod_{j=1}^D \mathcal{N}(\mu(j, :), \Sigma) = \prod_{j=1}^D \mathcal{N}(\partial \mathbf{K}_{\mathbf{z},*}^\top \mathbf{K}_{\mathbf{z},\mathbf{z}}^{-1} \mathbf{Y}_{:,j}, \partial^2 \mathbf{K}_{*,*} - \partial \mathbf{K}_{*,\mathbf{x}}^\top \mathbf{K}_{\mathbf{z},\mathbf{z}}^{-1} \partial \mathbf{K}_{*,\mathbf{z}}), \quad (4.2)$$

where we use standard notation for GPs [14]. It then follows that  $\mathbf{M}$  at a given point is governed by a non-central Wishart distribution [12]

$$D \cdot \mathbf{M} \sim \mathcal{W}_d(D, \Sigma, \Sigma^{-1} \mathbb{E}[\mathbf{J}]^\top \mathbb{E}[\mathbf{J}]). \quad (4.3)$$

The entire metric by definition follows a generalized Wishart process [22]. Note that a sample path from this process is smooth when the underlying covariance function  $k$  is smooth as well, and we have a proper distribution over Riemannian metrics. However, a sample from  $f$  gives a manifold that is only locally diffeomorphic to  $d$ -dimensional Euclidean space, and it may globally self-intersect.

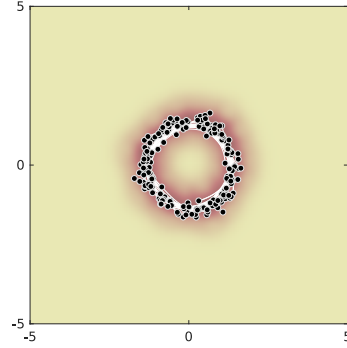


Figure 6: Geodesics for Gaussian process regression. The uncertainty force geodesics to move along the manifold.

Since the metric is a stochastic variable, we cannot apply standard Riemannian geometry to understand the space  $\mathcal{Z}$  (e.g. curvature is stochastic, geodesics are solutions to a stochastic differential equation, etc.). We can, however, inspect the leading moments of the metric

$$\mathbb{E}[\mathbf{M}] = \frac{1}{D} \mathbb{E}[\mathbf{J}^\top \mathbf{J}] = \frac{1}{D} \mathbb{E}[\mathbf{J}]^\top \mathbb{E}[\mathbf{J}] + \Sigma \quad (4.4)$$

$$\text{var}[M_{ij}] = \frac{1}{D} (\Sigma_{ij}^2 + \Sigma_{ii} \Sigma_{jj}) + \frac{1}{D^2} \mu_j^\top \Sigma \mu_j + \frac{1}{D^2} \mu_i^\top \Sigma \mu_i. \quad (4.5)$$

We note that  $\text{var}[M_{ij}] = \mathcal{O}(1/D)$  such that the variance of the metric vanishes in the limit  $D \rightarrow \infty$ . This can equivalently be seen from the central limit theorem. The metric, thus, becomes fully deterministic even if the underlying manifold is a stochastic object. This is a very useful result as it implies that we can well-approximate the stochastic metric with a deterministic metric, where computational tools are readily available.

To see if this approach can learn the geometric structure of the data manifold, we again consider the Gaussian kernel (3.6). Straight-forward calculations show that

$$\Sigma \xrightarrow{\text{near}} \mathbf{0} \quad \text{and} \quad \Sigma = \partial^2 \mathbf{K}_{*,*} - \partial \mathbf{K}_{*,\mathbf{x}}^\top \mathbf{K}^{-1} \partial \mathbf{K}_{*,\mathbf{x}} \xrightarrow{\text{away}} \alpha \theta_{\text{RBF}} \mathbf{I}, \quad (4.6)$$

where  $\alpha$  and  $\theta_{\text{RBF}}$  are the kernel parameters. From this we see that near the data, the expected metric (4.4) coincides with the true pull-back metric of the manifold (as in the deterministic setting),

$$\mathbb{E}[\mathbf{M}] \xrightarrow{\text{near}} \frac{1}{D} \mathbb{E}[\mathbf{J}]^\top \mathbb{E}[\mathbf{J}]. \quad (4.7)$$

In regions of  $\mathcal{Z}$  where there is no data, we have

$$\mathbb{E}[\mathbf{M}] \xrightarrow{\text{away}} \frac{1}{D} \mathbb{E}[\mathbf{J}]^\top \mathbb{E}[\mathbf{J}] + \alpha \theta_{\text{RBF}} \mathbf{I}. \quad (4.8)$$

If  $\alpha \theta_{\text{RBF}}$  is sufficiently large then geodesics will not go through regions of  $\mathcal{Z}$  where we do not have data. When data is sampled densely on the manifold, we often estimate large values of  $\alpha$  (corresponding to a small length-scale, i.e. a less smooth manifold), and a large penalty will be paid for “falling off the manifold”. To validate these observations, we return to our guiding example; Fig. 6 shows that geodesics under the expected metric (4.4) actually follow approximately circular arcs. This aligns with the theoretical analysis and demonstrates that, unlike a deterministic method, a probabilistic method can actually learn the differential geometric structure of a data manifold. This does, however, not provide us with any guarantees: we can only accurately learn the manifold geometry when data is sampled sufficiently dense on the manifold, but at least there is now hope, whereas the deterministic approaches are bound to fail.

**Discussion.** We see that deterministic methods can capture local geometry of the data manifold near the observed data, but they fail to capture the geometry where data is missing. This is not surprising, as we can generally only learn when we have data. What is, perhaps, more surprising is that if we can estimate the uncertainty of the manifold, then that translate directly into geometric information: if there is a hole in the manifold, then we can only see it through a lens of uncertainty. Not quantifying the uncertainty prevents us from seeing holes and boundaries of a data manifold. Uncertainty, thus, plays the same role as topology does in classic geometry, and this must also be estimated from data.

## 5 Bayesian geometry

Seeing that the expected metric actually has a chance of capturing the geometry of the data manifold, we now set out to get a better understanding of stochastic Riemannian metrics in the context of latent variable models. We here consider the case of the GP-LVM where  $f$  is a Gaussian process, and assume that the applied covariance function is at least twice differentiable, such that the derivative  $\dot{f} = \partial_t f$  is also a Gaussian process.

### 5.1 Detour: Euclidean geometry

Before getting a better understanding of stochastic Riemannian metrics, let us consider case of a stochastic Euclidean metric. That is, let  $\mathbf{u}, \mathbf{v} \in \mathbb{R}^d$  denote two deterministic vectors, and define their stochastic inner product as

$$\langle \mathbf{u}, \mathbf{v} \rangle = (\mathbf{A}\mathbf{u})^\top (\mathbf{A}\mathbf{v}) = \mathbf{u}^\top (\mathbf{A}^\top \mathbf{A}) \mathbf{v}, \quad (5.1)$$

where  $\mathbf{A} \in \mathbb{R}^{D \times d}$  is a random matrix with some distribution.

We first note that under this inner product, the shortest path between two points is the straight line connecting them. Here stochasticity does not change our usual geometric intuitions. The length of this shortest path is, however, stochastic. We can easily get a grasp of this length by defining  $\mathbf{x} = \mathbf{A}(\mathbf{u} - \mathbf{v})$  and noting that

$$\mathbb{E} [\|\mathbf{x}\|^2] = \sum_{j=1}^D \mathbb{E}[x_j^2] = \sum_{j=1}^D \{\mathbb{E}[x_j]^2 + \text{var}[x_j]\} = \mathbb{E}[\mathbf{x}]^\top \mathbb{E}[\mathbf{x}] + \text{tr}(\text{cov}[\mathbf{x}]). \quad (5.2)$$

We see that the expected distance between two points under a stochastic Euclidean metric depends on two terms: one that depends on the expected change of basis, and another that captures the variance of the basis. This tells us that expected distances are inherently large when the metric (or equivalently the new basis) has large variance.

**Example 1** (a Gaussian basis). Consider the case where each row of  $\mathbf{A}$  is drawn independently from the vector-valued distribution  $\mathcal{N}(\mathbf{0}, \Sigma)$ , such that the metric follows a Wishart distribution [12]

$$\mathbf{M} = \mathbf{A}^\top \mathbf{A} \sim \mathcal{W}_d(D, \Sigma). \quad (5.3)$$

From this we see that the squared distance from  $\mathbf{u}$  to  $\mathbf{v}$  also follows a Wishart distribution

$$\text{dist}^2(\mathbf{u}, \mathbf{v}) \sim \mathcal{W}_1(D, \sigma_{\mathbf{u}, \mathbf{v}}^2), \quad \sigma_{\mathbf{u}, \mathbf{v}}^2 = (\mathbf{u} - \mathbf{v})^\top \Sigma (\mathbf{u} - \mathbf{v}). \quad (5.4)$$

The square-root of this, then follows a Nakagami distribution [10]

$$\text{dist}(\mathbf{u}, \mathbf{v}) \sim \text{Nakagami}\left(\frac{D}{2}, D\sigma_{\mathbf{u}, \mathbf{v}}^2\right), \quad (5.5)$$

and the expected distance between two points is

$$\mathbb{E}[\text{dist}(\mathbf{u}, \mathbf{v})] = \frac{\Gamma(\frac{D+1}{2})}{\Gamma(\frac{D}{2})} \sqrt{2}\sigma_{\mathbf{u}, \mathbf{v}} \quad (5.6)$$

$$\propto \sigma_{\mathbf{u}, \mathbf{v}} = \sqrt{(\mathbf{u} - \mathbf{v})^\top \Sigma (\mathbf{u} - \mathbf{v})}. \quad (5.7)$$

In this simple example, we see that the expected distance is similar to the usual Mahalanobis' distance. We also note that if we scale the covariance matrix  $\Sigma$ , then we also scale the expected distance: *very uncertain metrics imply large expected distances*.

## 5.2 Geodesics

After this brief detour into Euclidean geometry, we return to the geometry of the GP-LVM. We first seek an understanding of the notion of shortest paths. Let  $\mathbf{c} : [a, b] \rightarrow \mathcal{Z}$  denote a deterministic differentiable curve, and let  $f(\mathbf{c})$  denote its stochastic embedding in  $\mathcal{X}$ . We stress that  $\mathbf{c}$  is a deterministic curve in  $\mathcal{Z}$ , while  $f(\mathbf{c})$  is a GP in  $\mathcal{X}$ .

The curve  $f(\mathbf{c})$  then has energy

$$\mathcal{E}(f(\mathbf{c})) = \frac{1}{2} \int_a^b \dot{\mathbf{c}}_t^\top \mathbf{M}_{\mathbf{c}_t} \dot{\mathbf{c}}_t dt. \quad (5.8)$$

This is a random quantity and it is natural to consider its expectation with respect to the random metric. Since the integrand is positive, Tonelli's Theorem tells us that this expected energy is

$$\bar{\mathcal{E}}(\mathbf{c}) \equiv \mathbb{E}_{\mathbf{M}}[\mathcal{E}(f(\mathbf{c}))] = \frac{1}{2} \mathbb{E}_{\mathbf{M}} \left[ \int_a^b \dot{\mathbf{c}}_t^\top \mathbf{M}_{\mathbf{c}_t} \dot{\mathbf{c}}_t dt \right] = \frac{1}{2} \int_a^b \dot{\mathbf{c}}_t^\top \mathbb{E}[\mathbf{M}_{\mathbf{c}_t}] \dot{\mathbf{c}}_t dt. \quad (5.9)$$

This implies that the curve  $\mathbf{c}$  with minimal expected energy over the stochastic manifold, is the geodesic under the deterministic Riemannian metric  $\mathbb{E}[\mathbf{M}]$ . This is exactly the geodesics considered in the previous section.



We can understand the curve minimizing expected energy in more explicit terms as follows. Let  $u_t = \mathbb{E}[\|\dot{\mathbf{c}}_t\|]$  and  $v_t = 1$  denote two functions over the interval  $[a, b]$ ; here we use the short-hand notation  $\|\dot{\mathbf{c}}_t\| = \sqrt{\dot{\mathbf{c}}_t^\top \mathbf{M}_{\mathbf{c}_t} \dot{\mathbf{c}}_t}$ . Then Cauchy-Schwartz's inequality tells us that

$$|\langle u, v \rangle|^2 \leq \|u\|^2 \cdot \|v\|^2 \quad (5.10)$$

$$\left( \int_a^b \mathbb{E}[\|\dot{\mathbf{c}}_t\|] dt \right)^2 \leq \int_a^b \mathbb{E}[\|\dot{\mathbf{c}}_t\|^2] dt \cdot \int_a^b dt = (b-a) \int_a^b \mathbb{E}[\|\dot{\mathbf{c}}_t\|^2] dt. \quad (5.11)$$

Letting

$$\bar{\mathcal{L}}(\mathbf{c}) = \mathbb{E} \left[ \int_a^b \|\dot{\mathbf{c}}_t\| dt \right] = \int_a^b \mathbb{E}[\|\dot{\mathbf{c}}_t\|] dt \quad (5.12)$$

denote the expected length of  $\mathbf{c}$  we then get

$$\int_a^b \mathbb{E}[\|\dot{\mathbf{c}}_t\|^2] dt \geq \frac{\bar{\mathcal{L}}^2(\mathbf{c})}{b-a}. \quad (5.13)$$

Equality is achieved when  $u_t$  and  $v_t$  are parallel, that is when  $\mathbb{E}[\|\dot{\mathbf{c}}_t\|]$  is constant. Since  $\mathbf{c}_t$  is a deterministic curve, we can always reparametrize it to have constant expected speed and achieve equality.

Using that  $\text{var}[x] = \mathbb{E}[x^2] - \mathbb{E}[x]^2$  we note that

$$\int_a^b \mathbb{E}[\|\dot{\mathbf{c}}_t\|^2] dt = \int_a^b \mathbb{E}[\|\dot{\mathbf{c}}_t\|^2] dt - \int_a^b \text{var}[\|\dot{\mathbf{c}}_t\|] dt = 2\bar{\mathcal{L}}(\mathbf{c}) - \int_a^b \text{var}[\|\dot{\mathbf{c}}_t\|] dt. \quad (5.14)$$

Assuming that the curve has been parametrized to have constant expected speed, we then get

$$\bar{\mathcal{E}}(\mathbf{c}) = \frac{\bar{\mathcal{L}}^2(\mathbf{c})}{2(b-a)} + \frac{1}{2} \int_a^b \text{var}[\|\dot{\mathbf{c}}_t\|] dt. \quad (5.15)$$

Minimizing expected curve energy, thus, does not always minimize the expected curve length. Rather, this balances the minimization of expected curve length and the minimization of curve variance.

**Implications and interpretation.** On a deterministic manifold, we know that minimizing curve energy results in a curve of minimal length (evident from Eq. 5.15 as the variance term vanishes). When the manifold is stochastic, we see that minimizing expected curve energy does not imply a minimization of expected curve length. In some sense, this is disappointing, but the revelation force us to consider the elementary question: *do we really want to traverse paths of minimal expected length?* If the path of minimal expected length has very large variance, do we still consider it a useful interpolant for two data points? One could even argue that the path of minimal variance is the most natural interpolant, even if this might not be the shortest path (in expectation). It is in this light, that Eq. 5.15 should be interpreted: it is an intriguing property of minimizing expected energy that this corresponds to minimizing a combination of length and variance. Since the expected energy minimizing curve is simply the geodesic under the expected Riemannian metric, this also lend itself to easy computation as we can use standard tools from deterministic Riemannian geometry. It is, however, worth exploring proper length minimization.

**Example 2** (a Gaussian process prior manifold). There are cases where expected energy and length are strongly related. As an example, consider the case where each dimension of  $f$  is a zero-mean Gaussian process with a sufficiently smooth covariance function. In the machine learning literature such processes are usually used for specifying priors. Let the distribution of the Jacobian of  $f$  at  $\mathbf{z}$  be given by

$$\mathbf{J}_{\mathbf{z}} \sim \prod_{j=1}^D \mathcal{N}(\mathbf{0}, \boldsymbol{\Sigma}_{\mathbf{z}}), \quad (5.16)$$

such that  $\mathbf{J}_{\mathbf{z}}^\top \mathbf{J}_{\mathbf{z}}$  follows a Wishart distribution,

$$D \cdot \mathbf{M}_{\mathbf{z}} = \mathbf{J}_{\mathbf{z}}^\top \mathbf{J}_{\mathbf{z}} \sim \mathcal{W}_d(D, \boldsymbol{\Sigma}_{\mathbf{z}}). \quad (5.17)$$

The expected energy of a curve  $\mathbf{c} : [a, b] \rightarrow \mathcal{Z}$  is then

$$\bar{\mathcal{E}}(\mathbf{c}) = \frac{1}{2} \int_a^b \mathbb{E} [\dot{\mathbf{c}}_t^\top \mathbf{M}_{\mathbf{c}_t} \dot{\mathbf{c}}_t] dt = \frac{D}{2} \int_a^b \dot{\mathbf{c}}_t^\top \boldsymbol{\Sigma}_{\mathbf{c}_t} \dot{\mathbf{c}}_t dt \quad (5.18)$$

since  $\dot{\mathbf{c}}_t^\top \mathbf{M}_{\mathbf{c}_t} \dot{\mathbf{c}}_t \sim \mathcal{W}_1(D, \dot{\mathbf{c}}_t^\top \boldsymbol{\Sigma}_{\mathbf{c}_t} \dot{\mathbf{c}}_t)$ . Following the derivations in Example 1 we see that the expected length of  $\mathbf{c}$  is

$$\bar{\mathcal{L}}(\mathbf{c}) \propto \int_a^b \sqrt{\dot{\mathbf{c}}_t^\top \boldsymbol{\Sigma}_{\mathbf{c}_t} \dot{\mathbf{c}}_t} dt. \quad (5.19)$$

We can then interpret  $\boldsymbol{\Sigma}_{\mathbf{z}}$  as a Riemannian metric and note that the expressions for curve length and energy under this metric exactly correspond to Eqs. 5.19 and 5.18. By Proposition 1, we then have that minimizing expected curve energy also minimize expected curve length.

### 5.3 Integration

Let  $\Omega \subseteq \mathcal{Z}$  such that  $f(\Omega) \subseteq \mathcal{M}$ , and let  $h : f(\Omega) \rightarrow \mathbb{R}$  denote a real-valued integratable function over the specified part of the manifold. We now seek its integral over the entire domain under a random Riemannian metric  $\mathbf{M}$ . That is,

$$\bar{h} = \int_{f(\Omega)} h(\mathbf{x}) d\mathbf{x} = \int_{\Omega} h(f(\mathbf{z})) \sqrt{\det \mathbf{M}_{\mathbf{z}}} d\mathbf{z}. \quad (5.20)$$

Since the metric is stochastic, then so is  $\bar{h}$ . We evaluate its expectation as

$$\mathbb{E}_{\mathbf{M}}[\bar{h}] = \mathbb{E}_{\mathbf{M}} \left[ \int_{\Omega} h(f(\mathbf{z})) \sqrt{\det \mathbf{M}_{\mathbf{z}}} d\mathbf{z} \right] \quad (5.21)$$

$$= \int_{\Omega} h(f(\mathbf{z})) \mathbb{E} \left[ \sqrt{\det \mathbf{M}_{\mathbf{z}}} \right] d\mathbf{z}. \quad (5.22)$$

That is, the integration is simply performed under the expected volume measure (as expected).

The variance of the integral can be expressed as

$$\text{var} [\bar{h}] = \mathbb{E} [\bar{h}^2] - \mathbb{E} [\bar{h}]^2, \quad (5.23)$$

where the last term easily is computed from Eq. 5.22. The missing term is

$$\mathbb{E} [\bar{h}^2] = \mathbb{E}_{\mathbf{M}} \left[ \left( \int_{\Omega} h(f(\mathbf{z})) \sqrt{\det \mathbf{M}_{\mathbf{z}}} d\mathbf{z} \right)^2 \right], \quad (5.24)$$

which generally does not permit a closed-form expression. When  $\Omega$  is a finite domain, the following bound (due to Cauchy-Schwarz) may be useful

$$\mathbb{E} [\bar{h}^2] \leq \mathbb{E}_{\mathbf{M}} \left[ \int_{\Omega} (h(f(\mathbf{z})) \sqrt{\det \mathbf{M}_{\mathbf{z}}})^2 d\mathbf{z} \int_{\Omega} d\mathbf{z} \right] \quad (5.25)$$

$$= \int_{\Omega} (h(f(\mathbf{z})))^2 \mathbb{E} [\det \mathbf{M}_{\mathbf{z}}] d\mathbf{z} \int_{\Omega} d\mathbf{z}. \quad (5.26)$$

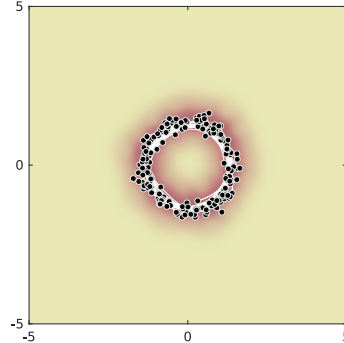


Figure 7: As Fig. 6, but with the expected volume measure as background.

As stated above, this is only potentially useful when  $\Omega$  is finite, as otherwise Eq. 5.26 is infinite. In general, we do not have useful expressions for evaluating the variance of the integral  $\bar{h}$ .

We have previously seen that geodesics under the expected metric are well-behaved, so it is tempting to treat the manifold as having a deterministic metric. From an integration point-of-view this implies working with the measure  $\sqrt{\det(\mathbb{E}[\mathbf{M}_{\mathbf{z}}])}$ . This is notably different than the expected measure,  $\mathbb{E}[\sqrt{\det \mathbf{M}_{\mathbf{z}}}]$ , implied by the above analysis, and one should be aware that this choice could have a subtle influence on integrals.

**Example 3** (a Gaussian process prior manifold). There are cases where the choice of measure is of less importance. To see this, we return to the Gaussian process prior manifold of Example 2. As before, the metric at  $\mathbf{z}$  follows a (scaled) Wishart distribution,

$$D \cdot \mathbf{M}_{\mathbf{z}} = \mathbf{J}_{\mathbf{z}}^{\top} \mathbf{J}_{\mathbf{z}} \sim \mathcal{W}_d(D, \boldsymbol{\Sigma}_{\mathbf{z}}). \quad (5.27)$$

Theorem 3.2.15 of Muirhead's book [12] tells us that

$$\mathbb{E} \left[ \sqrt{\det(D\mathbf{M}_{\mathbf{z}})} \right] = \sqrt{\det \boldsymbol{\Sigma}_{\mathbf{z}}} 2^{d/2} \frac{\Gamma\left(\frac{D+1}{2}\right)}{\Gamma\left(\frac{D-d+1}{2}\right)} \Leftrightarrow \quad (5.28)$$

$$\mathbb{E} \left[ \sqrt{\det(\mathbf{M}_{\mathbf{z}})} \right] \propto \sqrt{\det \boldsymbol{\Sigma}_{\mathbf{z}}}. \quad (5.29)$$

The measure associated with the expected metric is

$$\sqrt{\det \mathbb{E}[\mathbf{M}_{\mathbf{z}}]} = \sqrt{\det \boldsymbol{\Sigma}_{\mathbf{z}}} \quad (5.30)$$

and we conclude that for this prior manifold, the two measures are proportional.

**Example 4** (the GP-LVM). Things are not as simple when considering the posterior GP-LVM manifold. Here the (scaled) metric at  $\mathbf{z}$  follows a non-central Wishart distribution

$$D \cdot \mathbf{M} \sim \mathcal{W}_d(D, \boldsymbol{\Sigma}_{\mathbf{z}}, \boldsymbol{\Sigma}_{\mathbf{z}}^{-1} \mathbb{E}[\mathbf{J}]^{\top} \mathbb{E}[\mathbf{J}]). \quad (5.31)$$

By Theorem 10.3.7 of Muirhead's book [12] we get that

$$\mathbb{E} \left[ \sqrt{\det(D\mathbf{M}_{\mathbf{z}})} \right] = \frac{2^{d/2}}{\pi D^{d/2}} \frac{\Gamma\left(\frac{D+2}{4}\right)}{\Gamma\left(\frac{D-d+2}{4}\right)} \quad (5.32)$$

$${}_1F_1\left(-1/2, D/2, -1/2 \boldsymbol{\Sigma}_{\mathbf{z}}^{-1} \mathbb{E}[\mathbf{J}]^{\top} \mathbb{E}[\mathbf{J}]\right) \sqrt{\det \boldsymbol{\Sigma}_{\mathbf{z}}},$$

where  ${}_1F_1$  is the confluent hypergeometric function of the first kind. On the other hand, the measure associated with the expected metric is

$$\sqrt{\det \mathbb{E}[\mathbf{M}_{\mathbf{z}}]} = \sqrt{\det (1/D \mathbb{E}[\mathbf{J}_{\mathbf{z}}]^{\top} \mathbb{E}[\mathbf{J}_{\mathbf{z}}] + \boldsymbol{\Sigma}_{\mathbf{z}})} \quad (5.33)$$

and we see that the two measures appear quite different. To understand this difference in practice, we show the volume measure of the expected metric (5.33) in the background of Fig. 6. Similarly, we show the expected volume measure (5.32) in Fig. 7. Somewhat surprisingly, there is no visual difference between the two different measures. This indicates that for the GP-LVM, the more simple volume measure associated with the expected metric is a good approximation to the expected volume measure.

## 6 Deep generative models

So far, our discussion has centered around kernel based methods as these are fairly easy to understand theoretically. The key observations, however, generally holds true, and we move on to consider more modern approaches based on neural networks.

## 6.1 The deterministic setting

The natural case is to estimate  $f$  with a (potentially deep) feed-forward neural network. We shall call this case an *autoencoder* as these classic methods are the prime example of such an architecture. When we consider the associated pull-back metric, then the same considerations hold true as in the kernel-based setting (Sec. 3.2). That is, if we regularize towards a smooth  $f$ , then geodesics will naturally cross through holes in the data manifold. To validate this, we return to our guiding example (Sec. 3.1). Figure 8 shows that the implied geodesics are almost straight lines. This is to be expected as we are considering a deterministic approach, and these are fundamentally incapable of learning the manifold topology.

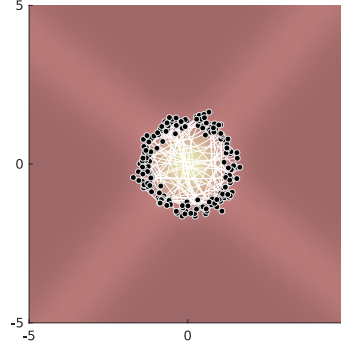


Figure 8: Geodesics for an autoencoder, i.e.  $f$  is a sufficiently smooth feed-forward network.

## 6.2 The Bayesian setting

With the advent of variational autoencoders [8, 15] came the idea of probabilistic mappings  $f$  represented by two neural networks, one for the mean and one for the (Gaussian) uncertainty. That is, in these models we represent  $f$  as

$$f(\mathbf{z}) = \boldsymbol{\mu}(\mathbf{z}) + \boldsymbol{\sigma} \odot \boldsymbol{\epsilon}, \quad \boldsymbol{\epsilon} \sim \mathcal{N}(\mathbf{0}, \mathbf{I}_D), \quad (6.1)$$

where  $\boldsymbol{\mu}$  and  $\boldsymbol{\sigma}$  are neural networks,  $\odot$  is the element-wise (Hadamard) product, and  $\mathbf{I}_D$  is the  $D \times D$  identity matrix. This gives us a highly flexible way to parametrize uncertain mappings.

From a geometric perspective it is worth pointing out that under this choice of  $f$  the noise does not form a smooth process. As such, sample paths from  $f$  are not smooth, and one can question the validity of pull-back metrics of this model. If we proceed disregarding any such concerns, then it is easy to show that [1]

$$D \cdot \mathbb{E}[\mathbf{M}_{\mathbf{z}}] = \left(\mathbf{J}_{\mathbf{z}}^{(\boldsymbol{\mu})}\right)^\top \left(\mathbf{J}_{\mathbf{z}}^{(\boldsymbol{\mu})}\right) + \left(\mathbf{J}_{\mathbf{z}}^{(\boldsymbol{\sigma})}\right)^\top \left(\mathbf{J}_{\mathbf{z}}^{(\boldsymbol{\sigma})}\right), \quad (6.2)$$

where  $\mathbf{J}_{\mathbf{z}}^{(\boldsymbol{\mu})}$  and  $\mathbf{J}_{\mathbf{z}}^{(\boldsymbol{\sigma})}$  are the Jacobians of  $\boldsymbol{\mu}$  and  $\boldsymbol{\sigma}$ , respectively. As before, the variance of the metric also goes to zero when  $D \rightarrow \infty$ . This follows directly from the central limit theorem. These observations can be taken as a hint that the expected metric is a reasonable geometric structure for  $\mathcal{Z}$ .

We now return to our guiding example. Following standard practice we let  $\boldsymbol{\mu}$  and  $\boldsymbol{\sigma}$  be smooth feed-forward neural networks. The left panel of Fig. 9 shows that geodesics in this model are almost straight lines and that the model failed to capture the geometry of the data manifold. This happens because  $\boldsymbol{\sigma}$  is a poor proxy for uncertainty [1]. When we model  $\boldsymbol{\sigma}$  with a feed-forward neural network, we implicitly assume that we can smoothly interpolate the uncertainty estimate we can recover at  $\mathbf{z}_{1:N}$ . But smooth interpolation of uncertainty is nonsensical.<sup>2</sup> To counter this issue, Arvanitidis et al. [1] suggest to model  $\boldsymbol{\sigma}^{-1}$  with a positive RBF network [13]. This heuristic ensure that uncertainty grows when we move away from the data. This is an ad hoc choice, but the center panel of Fig. 9 shows that it allows us to recover the geometry of the data manifold.

In Example 4, we saw that for the GP-LVM the measure associated with the expected metric was practically identical to the expected measure, even if their mathematical expressions are quite different. This does not appear to be the case for the variational autoencoder. The center panel of Fig. 9 shows the measure associated with the expected metric, while the right panel shows the expected measure (computed using sampling). These measures are quite different and it is not immediately clear which is to be preferred from a practical perspective. This is a problem that deserve further study.

## 7 Previous work

Pull-back metrics have been studied in mathematics at least since the seminal work of Gauss [6], and formed the initial foundation of Riemannian geometry. In the machine learning literature, these

<sup>2</sup>As a simple example, consider a dataset consisting of two very precise (low variance) temperature readings at the poles of our planet. If we, from this data, interpolate the temperature at the equator, then a smooth interpolation of the uncertainty would imply that we were very certain about our prediction.

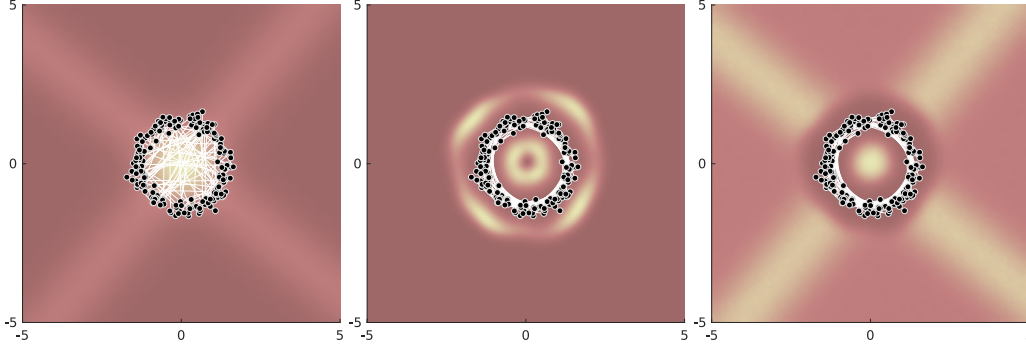


Figure 9: Geodesics for variational autoencoders. *Left*: a naive variational autoencoder, i.e. both mean and standard deviation of  $f$  are represented with smooth feed-forward networks. *Center*: Geodesics for a variational autoencoder with decaying precision, i.e. the mean of  $f$  is a smooth feed-forward network, while the inverse standard deviation of  $f$  is modeled with a positive RBF network. The background color is proportional to the measure of the expected metric. *Right*: same network as the center panel, but now the background color is proportional to the expected measure.

metrics have only been studied in few instances. To the best of our knowledge, Tosi et al. [21] was the first to give the latent space a geometric foundation. This was done in the context of the GP-LVM [11], but the discussion was quite general. Interestingly, Tosi et al. relied on the expected pull-back metric, and explicitly emphasized the importance of uncertainty. In that perspective, it is surprising that some more recent work (in the context of deep learning) disregard the uncertainty [19, 3, 9]. Shao et al. [19] and Chen et al. [3] consider pull-back metrics of variational autoencoders, but only consider the mean of  $f$ ; in our terminology they therefore consider particularly regularized autoencoders rather than variational autoencoders. Shao et al. note that most geodesics in their model are straight lines and speculate that this is because most data manifold are actually flat. Our analysis shows that this conclusion is most likely incorrect, and that the flatness is an artifact of disregarding uncertainty.

In parallel to Shao et al. [19] and Chen et al. [3], we [1] also considered pull-back metrics of variational autoencoders by taking the expected metric. We found significant curvature in data manifolds, which coincides with intuition.

## 8 Concluding remarks

The driving motivation for introducing pull-back metrics in the latent space of a generative model is to get rid of the arbitrariness in the choice of parametrization of the latent space. This is an important issue if we are to interpret the latent variables of a fitted model. We have argued that geometry provides a solution to the issue, but emphasize that this need not be the only solution. We have demonstrated that methods that do not quantify their own uncertainty cannot, in a meaningful way, capture the geometry of a data manifold. The key issue is that the usual smoothness assumptions imply that holes in the data manifold are interpolated so smoothly that geodesics are encouraged to pass through the holes rather than stay on the manifold. Methods that provide reasonable estimates of the uncertainty of the estimated manifold naturally avoid this issue as the uncertainty directly alters the estimated geometry. We find that uncertainty quantification in manifold learning end up playing the role of topology in classic geometry: uncertainty informs us about holes and boundaries in the manifold and provides us with a global notion of connectivity. Disregarding uncertainty, thus, imply disregarding the most important aspects manifold learning.

We have provided an extensive analysis of the geometry of the Gaussian latent variable model, and have developed elementary results for working with stochastic Riemannian manifolds. We have seen that minimizing expected curve energy on a stochastic manifold does not imply minimization of expected curve length, which forces us to reconsider which measure define the most natural interpolants.

Parts of our analysis can be extended to models based on neural networks. This raises two key issues for future research: 1) since sample paths from deep generative models are not continuous it is perhaps not a good idea to enforce a geometric analysis. It then becomes interesting to determine if

such smoothness can be introduced in deep generative models without sacrificing the computational efficiency of the models. 2) Uncertainty is essential for estimating the geometric structure of a data manifold, but unfortunately current deep generative models provide rather poor estimators of uncertainty. A heuristic from Arvanitidis et al. [1] seems to work reasonable well, but more elegant and robust methods would be of great value.

As a final note, we repeat the key point of the paper: *without uncertainty quantification, we cannot learn the geometric structure of a data manifold, and any attempt to do so is bound to fail beyond the most simple examples.*

## Acknowledgments

The author is grateful to Vagn Lundsgaard Hansen, Martin Jørgensen, Georgios Arvanitidis, and Aasa Feragen for enlightening discussions. SH was supported by a research grant (15334) from VILLUM FONDEN. This project has received funding from the European Research Council (ERC) under the European Union’s Horizon 2020 research and innovation programme (grant agreement n° 757360).

## References

- [1] G. Arvanitidis, L. K. Hansen, and S. Hauberg. Latent space oddity: on the curvature of deep generative models. In *International Conference on Learning Representations (ICLR)*, 2018.
- [2] M. Belkin and P. Niyogi. Laplacian Eigenmaps for Dimensionality Reduction and Data Representation. *Neural Computation*, 15(6):1373–1396, June 2003.
- [3] N. Chen, A. Klushyn, R. Kurle, X. Jiang, J. Bayer, and P. Smagt. Metrics for deep generative models. In *International Conference on Artificial Intelligence and Statistics*, pages 1540–1550, 2018.
- [4] D. L. Donoho and C. Grimes. Hessian eigenmaps: Locally linear embedding techniques for high-dimensional data. *Proceedings of the National Academy of Sciences*, 100(10):5591–5596, 2003. ISSN 0027-8424.
- [5] S. Gallot, D. Hulin, and J. Lafontaine. *Riemannian geometry*, volume 3. Springer, 1990.
- [6] C. F. Gauss. Disquisitiones generales circa superficies curvas. *Commentationes Societatis Regiae Scientiarum Gottingensis Recentiores*, VI:99–146, 1827.
- [7] F. Girosi, M. Jones, and T. Poggio. Regularization theory and neural networks architectures. *Neural computation*, 7(2):219–269, 1995.
- [8] D. P. Kingma and M. Welling. Auto-Encoding Variational Bayes. In *Proceedings of the 2nd International Conference on Learning Representations (ICLR)*, 2014.
- [9] S. Laine. Feature-based metrics for exploring the latent space of generative models, 2018. URL <https://openreview.net/forum?id=BJs1DBkWG>.
- [10] D. Laurenson. Nakagami distribution. *Indoor Radio Channel Propagation Modelling by Ray Tracing Techniques*, 1994.
- [11] N. D. Lawrence. Probabilistic non-linear principal component analysis with gaussian process latent variable models. *Journal of machine learning research*, 6(Nov):1783–1816, 2005.
- [12] R. J. Muirhead. *Aspects of Multivariate Statistical Theory*. John Wiley & Sons, 2005.
- [13] Q. Que and M. Belkin. Back to the future: Radial basis function networks revisited. In *Artificial Intelligence and Statistics (AISTATS)*, 2016.
- [14] C. E. Rasmussen and C. Williams. *Gaussian Processes for Machine Learning*. University Press Group Limited, 2006.
- [15] D. J. Rezende, S. Mohamed, and D. Wierstra. Stochastic backpropagation and variational inference in deep latent gaussian models. In *International Conference on Machine Learning*, volume 2, 2014.
- [16] S. T. Roweis and L. K. Saul. Nonlinear dimensionality reduction by locally linear embedding. *science*, 290(5500):2323–2326, 2000.
- [17] B. Schölkopf and A. J. Smola. *Learning with Kernels: Support Vector Machines, Regularization, Optimization, and Beyond*. MIT Press, 2001.

- [18] B. Schölkopf, A. Smola, and K.-R. Müller. Kernel principal component analysis. In *Advances in Kernel Methods - Support Vector Learning*, pages 327–352, 1999.
- [19] H. Shao, A. Kumar, and P. T. Fletcher. The riemannian geometry of deep generative models. *arXiv preprint arXiv:1711.08014*, 2017.
- [20] J. B. Tenenbaum, V. De Silva, and J. C. Langford. A global geometric framework for nonlinear dimensionality reduction. *science*, 290(5500):2319–2323, 2000.
- [21] A. Tosi, S. Hauberg, A. Vellido, and N. D. Lawrence. Metrics for Probabilistic Geometries. In *The Conference on Uncertainty in Artificial Intelligence (UAI)*, July 2014.
- [22] A. G. Wilson and Z. Ghahramani. Generalised wishart processes. In *Uncertainty in Artificial Intelligence (UAI)*, 2011.